Hindawi Publishing Corporation
International Journal of Antennas and Propagation
Volume 2016, Article ID 8180124, 10 pages
http://dx.doi.org/10.1155/2016/8180124

Research Article

Effect of Antenna Parameters on the Field Coverage in Tunnel Environments

Dawei Li[1,2] and Junhong Wang[1,2]

[1]*Key Laboratory of All Optical Network & Advanced Telecommunication Network of MOE, Beijing Jiaotong University, Beijing 100044, China*
[2]*Institute of Lightwave Technology, Beijing Jiaotong University, Beijing 100044, China*

Correspondence should be addressed to Dawei Li; 11111001@bjtu.edu.cn

Received 9 January 2016; Revised 13 March 2016; Accepted 12 April 2016

Academic Editor: Jose-Maria Molina-Garcia-Pardo

Radio wave propagation in confined spaces is consequent upon the reflections of boundaries; thus, the radiation characteristics of the antenna have significant influence on the field coverage in the confined space. This paper investigates the effects of antenna parameters on field coverage characteristics in a tunnel environment. A modified modal method is proposed to analyse the wave propagation properties along the tunnel. The relationships between the amplitudes of modes and the antenna parameters, including the beam width, beam direction, and antenna location, are analysed. The results indicate that by properly selecting the antenna parameters, optimum field coverage in tunnel environments can be realized.

1. Introduction

Effective and reliable electromagnetic wave coverage in confined environments is important to the quality of wireless communications. In general, the discrete antenna system and the leaky coaxial cable (LCX) system are two types of infrastructure widely used to generate wave coverage in confined spaces [1, 2]. The discrete antenna system is more flexible and efficient and is less expensive compared with the LCX system. However, most available discrete antennas suffer from unsatisfying performance, which may result in the interruption of communications in long and narrow confined areas, such as tunnels [3]. To overcome this shortcoming, the characteristics of the wave coverage generated by discrete antennas in tunnels should be investigated.

Radio propagation in tunnels has been studied for decades. Different types of methods have been employed to predict the propagation characteristics. Due to the bounding effect of the tunnel walls, the propagation characteristics in tunnels are different from those in open space. In [4, 5], the theoretical modal analysis is applied to build the propagation model, which has high accuracy when the receiver is far away from the transmitter. Nevertheless, the method has difficulty in taking the antenna parameters into account. The ray tracing method [6, 7] is another powerful way to address radio propagation in complex environments. The antenna parameters can be considered in this method, but it is difficult to explain the physical mechanism of the propagation procedure directly. Full wave calculation methods [8, 9], including finite difference time domain (FDTD), finite element method (FEM), and integral equations, can contain the effect of different antenna parameters, and precise results can be obtained. However, these methods are time and memory consuming for large-scale problems. Recently, the parabolic equation method [10, 11] has become popular in solving the radio propagation in tunnels as it can determine the path loss and fading characteristics in long tunnel environments in an acceptable amount of time. However, in applying this method, it is difficult to accurately model high order modes, especially in the vicinity of the transmitting antenna.

By using these reported methods, channel parameters, which are essential in wireless communication applications, including path loss, time delay, and break point, can be studied. In [4, 5], the field composition and propagation constants of the modes in a hollow rectangular dielectric waveguide were investigated. The propagation characteristics in the tunnel and the relationship between the beak point and the operating frequency, antenna gain, and dimensions of the

tunnel were analysed in [12]. However, most available studies generally consider the antenna and the wave propagation independently. According to the results in [13–15], the wave propagation is influenced by the properties of the antennas used in a confined space [13–15].

In this paper, the field coverage instead of wave propagation is used to describe the wave characteristics in tunnels where the antenna is located. As described in [16], the ray tracing method is mathematically equivalent to the modal method in the simulation of radio propagation in straight rectangular tunnels. However, the modal method in [16] is derived based on an isotropic source, which means that it is not suitable for the case of directional antennas. Hence, a modified modal method is proposed in this paper. By applying this method, the effects of antenna parameters (beam width, beam direction, and location of antennas) on the field coverage in tunnels can be successfully studied. The results achieved in this paper are valuable for the design of antennas to be used in confined spaces. Additionally, the amplitudes of the modes can be obtained, which is helpful in analysing the mechanism of field coverage.

The rest of this paper is organized as follows: in Section 2, the novel modal method is depicted in detail; in Section 3, the effect of antenna parameters on field coverage is presented; and, in Section 4, the conclusions are summarized.

2. Methodology

The model and parameters of the straight hollow rectangular tunnel considered in this paper are shown in Figure 1. The tunnel is directed along the $+z$-axis, and the origin of the coordinates is located in the centre of the tunnel cross section. Based on the ray tracing theory, the electric field at the point (x, y, z) in the tunnel can be expressed by the summation of the rays radiated by all the images of the source [17]:

$$E_r(x,y,z) = E_t \frac{1}{r_{m,n}} \sum_{m=-\infty}^{\infty} \sum_{n=-\infty}^{\infty} f(\theta,\varphi)\, e^{-jkr_{m,n}} \rho_{\perp}^{|m|} \rho_{\parallel}^{|n|}. \quad (1)$$

In the above equation, E_t is the magnitude of the transmitted electric field, k is the wave number, $r_{m,n}$ is the distance between the receiver and the image $I_{m,n}$, and $r_{m,n}$ is expressed by

$$r_{m,n} = \sqrt{(x_m - x)^2 + (y_n - y)^2 + z^2}, \quad (2)$$

where $x_m = 2ma + (-1)^m x_0$ and $y_n = 2nb + (-1)^n y_0$. x_0 and y_0 are the coordinates of the centre of the transmitting antenna in the $z = 0$ plane. It should be noted that only the case with vertical polarization is considered in this paper. $\rho_{\perp,\parallel}$ in (1) represents the reflection coefficients on the perpendicular and parallel walls, respectively, and can be calculated approximately by [17]

$$\rho_{\perp,\parallel} \approx -\exp\left(-\frac{2\cos\theta_{\perp,\parallel}}{\Delta_{\perp,\parallel}}\right), \quad (3)$$

where $\theta_{\perp} = \arccos(|x_m - x|/r_{m,n})$ and $\theta_{\parallel} = \arccos(|y_n - y|/r_{m,n})$ are the reflection angles on the perpendicular and parallel walls, respectively; $\Delta_{\perp,\parallel}$ is the quantity related to the effective surface impedance defined by $\Delta_{\perp} \approx \sqrt{\bar{\varepsilon}_a - 1}$, $\Delta_{\parallel} \approx \sqrt{\bar{\varepsilon}_b - 1}/\bar{\varepsilon}_b$; and $\bar{\varepsilon}_{a,b}$ are the complex relative permittivities of the vertical and horizontal walls, respectively.

$f(\theta, \varphi)$ in (1) represents the antenna radiation pattern. To simulate the radiation properties of the antenna, the Gaussian pattern is used as the excitation in this paper, which is given by

$$f(\theta,\varphi) = \exp\left[-\frac{(\theta-\theta_0)^2}{\sigma\theta_{\mathrm{BW}}^2} - \frac{(\varphi-\varphi_0)^2}{\sigma\varphi_{\mathrm{BW}}^2}\right], \quad (4)$$

where θ_0 and φ_0 represent the beam angles in the azimuth and elevation directions, respectively, θ_{BW} and φ_{BW} represent the beam widths in the azimuth and elevation directions, respectively, and σ is a constant equal to 0.7213. Because the tunnel is set along the $+z$ direction, the range of θ and φ in the forward direction is $(-\pi/2, \pi/2)$, and when the tunnel is sufficiently long, they can be approximated as

$$\varphi = \frac{(x_m - x)}{r_{m,n}}, \qquad \theta = \frac{(y_n - y)}{r_{m,n}}. \quad (5)$$

Then, (1) can be rewritten as

$$E_r(x,y,z) = \frac{E_t}{r_{m,n}} \cdot \sum_{m=-\infty}^{\infty} \sum_{n=-\infty}^{\infty} \exp\left\{-\left[\frac{(x_m - x)/r_{m,n} - \varphi_0}{\sqrt{\sigma}\varphi_{\mathrm{BW}}}\right]^2 - \left[\frac{(y_n - y)/r_{m,n} - \theta_0}{\sqrt{\sigma}\theta_{\mathrm{BW}}}\right]^2 - jkr_{m,n} - \frac{2|m|\,|x_m - x|}{r_{m,n}\Delta_{\perp}} - \frac{2|n|\,|y_n - y|}{r_{m,n}\Delta_{\parallel}}\right\}. \quad (6)$$

Similar to that in [16], (6) can be written as

$$E_r(x,y,z) = \sum_{s_1=-\infty}^{\infty} \sum_{s_2=-\infty}^{\infty} \sum_{l=1}^{4} (-1)^{l+1} f_l(t_1, t_2), \quad (7)$$

where $t_1 = x_m - x$, $t_2 = y_n - y$, $s_1 = (t_1 - \bar{x}_l)/4a$, and $s_2 = (t_2 - \bar{y}_l)/4b$. $\bar{x}_l = x_0 - x$ and $\bar{y}_l = y_0 - y$ for even numbers of m and n, respectively, and $\bar{x}_l = 2a - x_0 - x$ and $\bar{y}_l = 2b - y_0 - y$

for odd numbers of m and n, respectively. For the case in this paper, $f_l(t_1, t_2)$ is expressed as

$$\begin{aligned} f_l(t_1,t_2) &= \frac{1}{\sqrt{t_1^2+t_2^2+z^2}} \\ &\cdot \exp\left\{-\left[\frac{t_1/\sqrt{t_1^2+t_2^2+z^2}-\varphi_0}{\sqrt{\sigma}\varphi_{\mathrm{BW}}}\right]^2\right. \\ &-\left[\frac{t_2/\sqrt{t_1^2+t_2^2+z^2}-\theta_0}{\sqrt{\sigma}\theta_{\mathrm{BW}}}\right]^2 \\ &-\frac{\left(\left|t_1\left(t_1-\widetilde{x}_l\right)\right|/a\Delta_\perp+\left|t_2\left(t_2-\widetilde{y}_l\right)\right|/b\Delta_\parallel\right)}{\sqrt{t_1^2+t_2^2+z^2}} \\ &\left.-jk\sqrt{t_1^2+t_2^2+z^2}\right\}. \end{aligned} \tag{8}$$

The definitions of the variables in (8) are the same as those defined in [16].

The Poisson Summation Formula (PSF) and saddle-point method can be utilized to convert (7) into the mode formula [16, 18], and then (7) can be expressed as

$$\begin{aligned} E_r(x,y,z) &= \frac{E_t\pi^2}{4ab}\sum_{p=-\infty}^{\infty}\sum_{q=-\infty}^{\infty}\sum_{l=1}^{4}(-1)^{l+1}\widetilde{f}_l\left(\frac{p\pi}{2a},\frac{q\pi}{2b}\right) \\ &\cdot e^{j((p\pi/2a)\overline{x}_l+(q\pi/2b)\overline{y}_l)}, \end{aligned} \tag{9}$$

where

$$\begin{aligned} \widetilde{f}_l(p,q) &\approx \frac{1}{j2\pi k\left(k^2-p^2-q^2\right)} \\ &\cdot \exp\left\{-\left[\frac{(p/k-\varphi_0)}{\sqrt{\sigma}\varphi_{\mathrm{BW}}}\right]^2-\left[\frac{(q/k-\theta_0)}{\sqrt{\sigma}\theta_{\mathrm{BW}}}\right]^2\right. \\ &-\left[\frac{1}{a\Delta_\perp}\left(\frac{p}{k}\right)^2+\frac{1}{b\Delta_\parallel}\left(\frac{p}{k}\right)^2\right]z \\ &\left.-jz\sqrt{k^2-p^2-q^2}\right\} \end{aligned} \tag{10}$$

and k is the wave number of free space. p and q are mode numbers corresponding to the horizontal and vertical directions, respectively. As derived in the Appendix, (9) can be simplified to

$$\begin{aligned} E_r(x,y,z) &= -\frac{j2\pi}{ab}\sum_{p=-\infty}^{\infty}\sum_{q=-\infty}^{\infty}A_{pq} \\ &\cdot\frac{e^{-(\alpha_{pq}+j\beta_{pq})z}}{\beta_{pq}}\sin\left(\frac{p\pi}{2a}x-\frac{p\pi}{2}\right)\sin\left(\frac{q\pi}{2b}y-\frac{q\pi}{2}\right). \end{aligned} \tag{11}$$

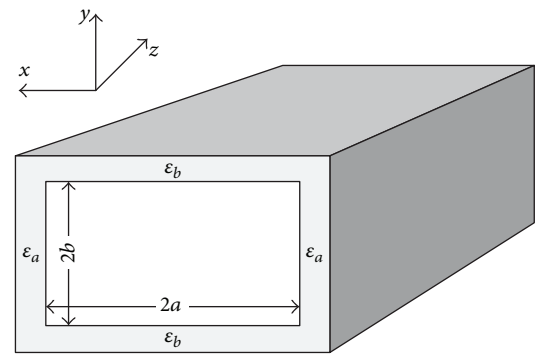

Figure 1: Geometry and parameters of a rectangular tunnel.

Note that (11) is exactly the weighted summation of the eigenfunctions of the propagation modes, where

$$\alpha_{pq} = \frac{1}{b}\left(\frac{q\lambda}{4b}\right)^2\frac{\overline{\varepsilon}_b}{\sqrt{\overline{\varepsilon}_b-1}}+\frac{1}{a}\left(\frac{p\lambda}{4a}\right)^2\frac{1}{\sqrt{\overline{\varepsilon}_a-1}}, \tag{12}$$

$$\beta_{pq} = \sqrt{k^2-\left(\frac{p\pi}{2a}\right)^2-\left(\frac{q\pi}{2b}\right)^2} \tag{13}$$

are the classic modal attenuation and propagation constants [4, 5]. The weight coefficients in (11) can be expressed as

$$\begin{aligned} A_{pq} &= \exp\left[-\frac{\theta_0^2+(p\pi/2ak)^2}{\sigma\theta_{\mathrm{BW}}^2}-\frac{\varphi_0^2+(q\pi/2bk)^2}{\sigma\varphi_{\mathrm{BW}}^2}\right] \\ &\cdot\sin\left(\frac{p\pi}{2a}x_0-\frac{p\pi}{2}-j\frac{p\pi\theta_0}{\sigma ak\theta_{\mathrm{BW}}^2}\right) \\ &\cdot\sin\left(\frac{q\pi}{2b}y_0-\frac{q\pi}{2}-j\frac{q\pi\varphi_0}{\sigma bk\varphi_{\mathrm{BW}}^2}\right). \end{aligned} \tag{14}$$

From (14), it is observed that the weight of each eigenfunction is exactly the mode amplitude A_{pq} in the excitation plane, and it is related to the beam width of the antenna, azimuth and elevation angles of the beam, and the location of the antenna. Hence, the effect of the antenna parameters on the radio propagation and field coverage characteristics can be analysed by modes. In actuality, all the antenna radiation patterns $F(\theta,\varphi)$ can be taken into account in rectangular tunnels by utilizing this method, indicating that the radiation pattern can be analytically expressed. The excitation mode amplitude can be expressed as

$$\begin{aligned} A_{pq} &= \left[\left(F_- - F_+\right)\cos\left(\frac{p\pi}{2a}x_0+\frac{q\pi}{2b}y_0-p\pi\right)\right. \\ &\left.-j\left(F_- + F_+\right)\sin\left(\frac{p\pi}{2a}x_0+\frac{q\pi}{2b}y_0-p\pi\right)\right], \end{aligned} \tag{15}$$

where F_+ represents $F(p\pi/2ak, q\pi/2bk)$ and F_- represents $F(-p\pi/2ak, -q\pi/2bk)$.

In this paper, the Gaussian radiation pattern is used as a special case to demonstrate the efficiency of the method. Figures 2(a) and 2(b) give the comparison between the

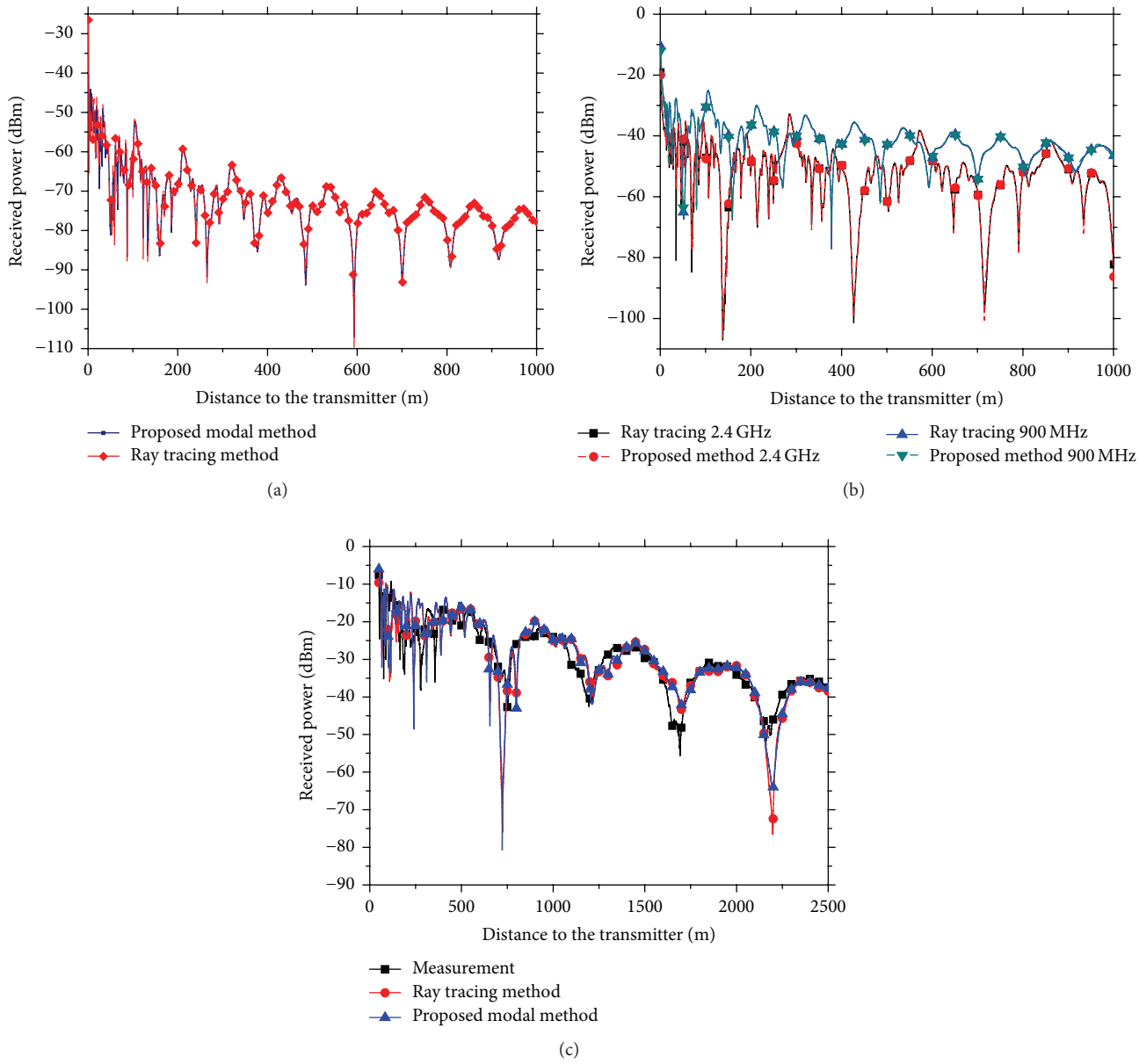

Figure 2: Comparison of the received power curves obtained by different methods with measurement of (a) the azimuth and elevation angles of antenna beam are 30°, and beam width is 15°; (b) comparison of the received power obtained by the proposed modal method with the measurement result in the Massif Central tunnel [20]; and (c) comparison of the received power at different frequencies obtained by the proposed method and ray tracing method.

received powers obtained with different beam tilt angles and frequencies using the modified modal method proposed in this paper and the ray tracing method, respectively. In the calculation, the transmitting antenna is located in the centre of the cross section of the tunnel with dimensions of 6 m × 6 m × 1000 m and an operating frequency of 900 MHz. The received power is calculated by [19]

$$P_r = \frac{3\lambda^2 E^2}{8\pi\eta_0}, \tag{16}$$

where E is the received field by a vertical polarized half wave dipole, η_0 is the wave impedance of free space, and λ is the wavelength. To ensure the accuracy of the approximation, the maximum orders of p and q in the modal method are set to 40. As shown in Figure 2, the result obtained from the new modal method agrees well with that of the ray tracing method. To further clarify the accuracy of the proposed modal method, the measured result in [20] is compared with that of this method. As shown in Figure 2(c), the result of the new modal method agrees well with the result measured in the Massif Central tunnel. The dimensions of the equivalent rectangle, which are suitable for simulating this tunnel, are listed in Table 1.

Table 1: Tunnel parameters.

Tunnel type	A	B	C	Tunnel in [20]
Width (m)	6	8	6	7.8
Height (m)	6	6	8	5.3
ε_r	6.8	6.8	6.8	5
σ (S/m)	3.4×10^{-2}	3.4×10^{-2}	3.4×10^{-2}	1×10^{-2}

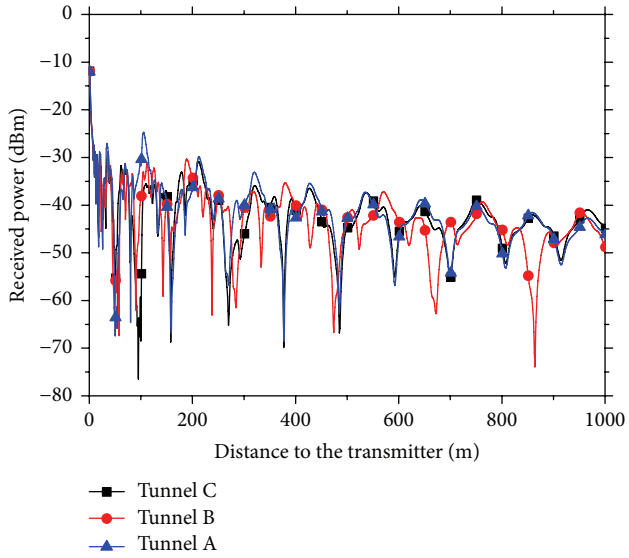

Figure 3: Comparison of the received power curves tested in different tunnels with the proposed modal method.

3. Results and Analysis

In this section, the effect of antenna parameters on the received power along a rectangular tunnel is analysed by utilizing the above modified modal method. The rectangular tunnels in this paper are set along the $+z$ direction, and the parameters of the tunnels are listed in Table 1. The relative permittivity and conductivity of the tunnel wall are shown in Table 1, which imitate the concrete. It is assumed that the antenna efficiency is 100% and the operating frequency is 900 MHz. The transmitting and receiving antennas are all vertically polarized.

3.1. Effect of Tunnel Dimensions. The curves of received power in tunnels A, B, and C are shown in Figure 3. To obtain the general rule of the effect of the tunnel dimension parameters on the field coverage characteristics, the transmitter and receiver are located in the centre of the cross section of the tunnels. From Figure 3, it is observed that the variations of the received power in the tunnels with the same width are similar. This similarity is because in the vertical polarization case, the dominant propagation modes are EH_{p1} modes, and the phase constants of those modes are related to the tunnel width. Thus, if the tunnel width is fixed, the superposed manner of the modes is the same. If the tunnel widths are different, the positions of peaks and nulls on the variation curves of the received power are changed, and the pseudo-periodicities become larger.

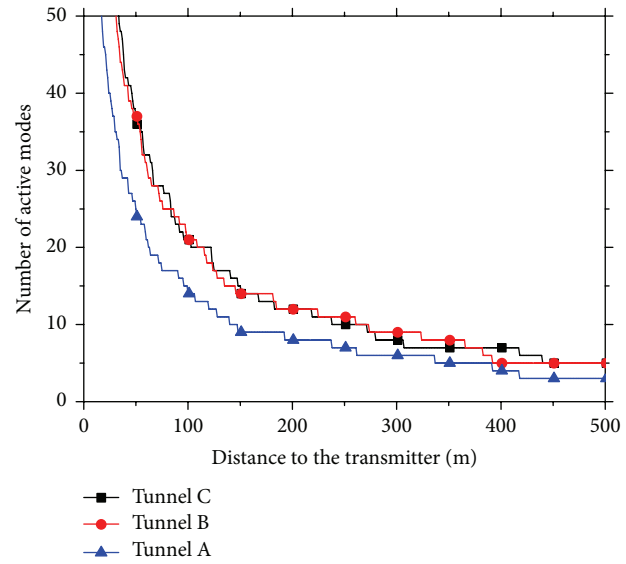

Figure 4: Comparison of the number of active modes tested in different tunnels with the proposed modal method.

In the tunnels, the number of modes, which significantly affects the received power, is an important parameter for interpreting the field coverage characteristics. The number of "active" modes, N_a (10%), is defined as the number of modes with power equal to at least 10% of the power in the most powerful mode [21]. The variations of N_a versus distance when transmitter is in the centre of the different tunnels are shown in Figure 4. The number of active modes helps for interpreting the fast variations of the received power around its mean value. In a small tunnel, the number of active modes is much smaller than in a large tunnel (as shown in Figure 4), so less modes can be reserved in the propagation process and arrive at the far region. Therefore, due to the superposition of different modes, the received power in the small tunnel suffers from less fluctuation as shown in Figure 3.

3.2. Effect of the Beam Width on Field Coverage. Considering that a rectangular tunnel with a height of 6 mm and width of 8 mm is common in practice, tunnel B is taken as an example to analyse the effect of antenna parameters on the field coverage characteristics. To evaluate the effect of the antenna beam width on the received power, the antenna is located in the centre of the cross section of the tunnel and points to the axial direction of the tunnel. The beam width of the transmitting antenna is set to 15°, 30°, 45°, and 60°, respectively. Figure 5 shows the received powers along the tunnel axis for different beam widths. As shown in Figure 5, the curves of the received powers generally have similar shapes, but, in the near region, the received power fluctuates significantly, leading to large differences in terms of the shapes of the curves, whereas, in the far region, the fluctuations become smaller. It is also shown that a narrower beam width of the transmitting antenna leads to smaller

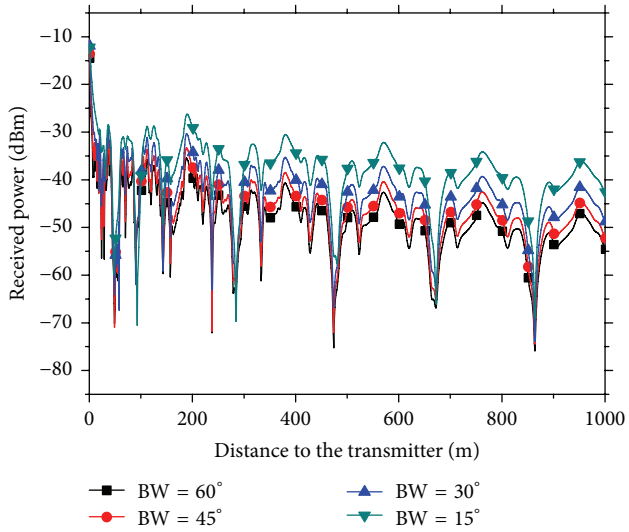

Figure 5: Variations of received powers along the tunnel axis for different antenna beam widths located in the centre of the cross section of tunnel, in which the azimuth and elevation angles of the antenna beam are 0°.

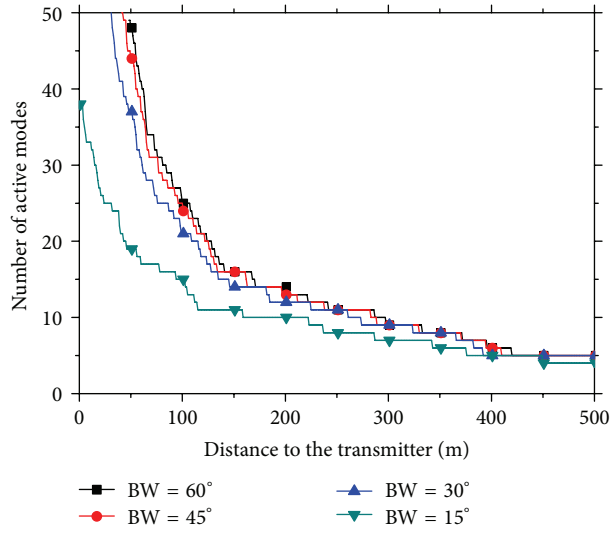

Figure 6: Comparison of the number of the active modes tested with different beam widths using the proposed modal method.

fluctuations in the near region and higher received power in the far region. In addition, the received power levels for different beam widths are similar to each other in the near region but significantly different in the far region. This phenomenon can be explained with the help of the proposed modal method. Figure 6 shows the variation of the number of active modes versus distance to the transmitter, which is excited by different antenna beam widths. It is shown that, for the narrower beam, the number of active modes is less, and the power is mainly transferred into the lower order modes. For the wider beam, the number of active modes is much higher than that of the narrower beam and more power is transferred into the higher order modes. From (12), it is obvious that the higher order modes have larger attenuation constants, so they decrease rapidly in the near region. Alternatively, for lower order modes, the attenuation constants are small, so they decline slowly. As a result, the received power for the wider beam presents rapid decay and deep fluctuation in the near region and becomes stable in the far region. This phenomenon can also be interpreted from Figure 6 in which the curve of the antenna with a beam width of 15° declines slowly, whereas the curve of the antenna with a beam width of 60° decreases rapidly. Thus, different mode compositions cause different received power distributions, which cannot be explained simply by the antenna gain. It is also noticed that increasing the number of active modes can improve the capacity of the diversity antenna systems, but it also reduces the received power level. Therefore, there is a trade-off between the number of active modes and the received power level.

In formula (14), there are two parameters, θ_0 and φ_0, related to the transmitting antennas. Because it is obvious that the antenna beam pointing to the tunnel axis exhibits the highest level, installing an antenna with a slightly tilted angle is a common method. Thus, θ_0 and φ_0 are usually fixed to 0°.

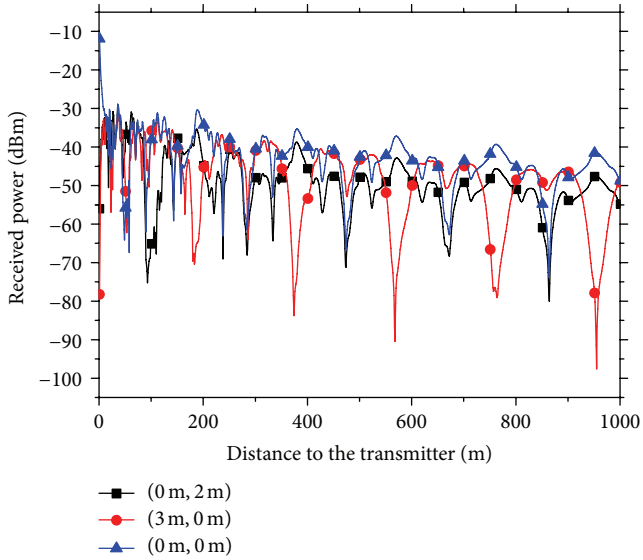

Figure 7: Variations of received powers along the tunnel axis for different antenna locations, in which the azimuth and elevation angles of the antenna beam are 0° and the antenna beam width is 30°.

3.3. Effect of Antenna Locations on Field Coverage. Many studies have investigated the effect of antenna position on the path loss characteristics from the angles of measurement or simulation [22, 23]. However, few studies consider this issue theoretically. Figure 7 shows the received power along the tunnel axis for different transverse locations of transmitting antenna in the tunnel cross section. It can be observed from Figure 7 that when the antenna moves vertically from the centre to the ceiling, the received power level reduces markedly, but the variation characteristic along the tunnel axis changes slightly. When the antenna moves horizontally from the centre to the side wall, the variation characteristic of

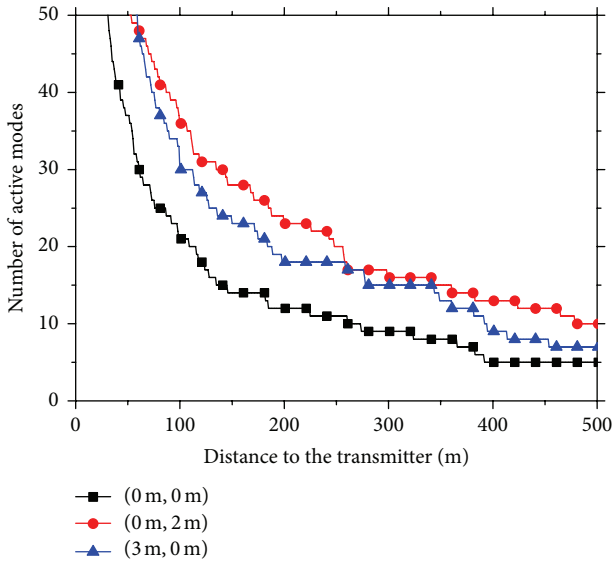

Figure 8: Comparison of the number of active modes tested with different antenna locations using the proposed modal method.

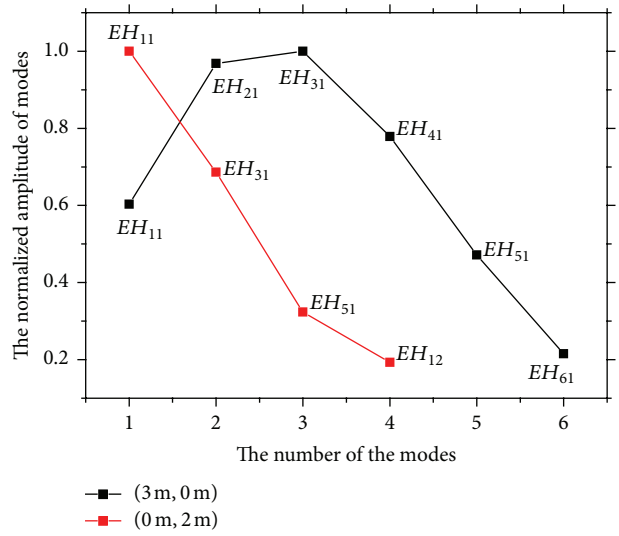

Figure 9: Comparison of the normalized amplitude distributions of active modes tested with different antenna locations in the plane of $z = 1000$ m using the proposed modal method.

Table 2: Active modes related to the transmitter location in the tunnel.

Distance to the Tx	$z = 100$ m	$z = 1000$ m
Transmitter location	(3 m, 0 m)	
Most powerful mode	EH_{31}	EH_{31}
Number of active modes	32	6
Transmitter location	(0 m, 2 m)	
Most powerful mode	EH_{13}	EH_{11}
Number of active modes	36	4

the received power along the tunnel axis changes significantly, and the positions of peaks and nulls markedly shift. When the transmitter is off centred, a large number of high order modes are excited and carry a large amount of energy. EH_{11} is not the mode with highest energy compared with these modes, different from the case of excitation by a centred transmitter. The high order modes rapidly attenuate in the process of propagation in the tunnel and take away a lot of energy, which is the reason why the received power level reduces markedly when the transmitter is off centre as shown in Figure 7.

Figure 8 shows three cases of the variation of the active mode number when the transmitting antenna is located in the centre, close to the side wall and to the ceiling, respectively. It can be found that when the transmitter is off centre many modes can be reserved in the tunnel compared with the case that transmitter is in the centre, which will result in the larger fluctuation of the received power.

To further understand the excited modes when the transmitter is located in different positions, Table 2 shows the order of the mode with the maximum amplitude in the planes of $z = 100$ and 1000. As Table 2 shows, when the antenna moves vertically to the ceiling, modes related to index q become significant. Because the high order modes with large q have larger attenuation constants, they rapidly decay along the tunnel, and finally only the fundamental modes remain in the far region. In contrast, when the antenna moves horizontally to the side wall, modes related to index p become significant, which have smaller attenuation constants, so many can be reserved in the propagation process and arrive at the far region. The normalized amplitude distributions of the active modes at the plane of $z = 1000$ m tested with different antenna locations are shown in Figure 9. When the transmitter moves horizontally, EH_{21}, EH_{41}, and EH_{61} are excited and can propagate for long distance, which cannot be excited when the transmitter move vertically. Therefore, due to the superposition of different modes, the received power for the case of the horizontally moving antenna suffers from larger fluctuation and deeper nulls, as shown in Figure 7. In addition, because the phase variations of modes for antennas moving horizontally are substantially different from those of antennas moving vertically, the locations of peaks and nulls change significantly.

From the above analysis, the effect of the antenna parameters (beam width and location) on the received power characteristics can be clearly observed. However, it is worth mentioning that the effects of these parameters are coupled together, and the effects should be considered simultaneously. According to the results, for the vertical polarization case, increasing the amplitudes of fundamental and lower order modes related to index p can extend the communication region in the tunnel. Because of the condition of practical application, the transmitting antenna has to be installed on the side wall. Thus, for the vertical polarization case, the narrow beam width antenna with no tilt or slight tilt is preferable.

From the above analysis, it can be found that by only changing the location of the transmitter it is hard to realize the optimum field coverage in the whole tunnel because deep fading along the tunnel still exists. Multitransmitters could realize the optimum field coverage in a line along the tunnel,

but not in the whole tunnel. Unlike multitransmitter systems, the spatial diversity system with multireceivers is an effective and flexible way to achieve uniform field coverage because it could utilize the irrelevance of the different positions of the tunnel to obtain an average level. Improving the diversity of antenna systems in tunnels, which has been a hot research topic in recent years [24, 25], is an efficient way to determine the optimal locations of transmitters and receivers to minimize the bit error rate and achieve higher capacity.

4. Conclusions

This paper investigates the field coverage characteristics in different tunnel environments for different antenna parameters, including beam width and antenna location. The analysis is based on a newly proposed, modified modal method, which is mathematically equivalent to the ray tracing method, for the simulation of the wave propagation in a tunnel environment. The relationship between the mode amplitudes and the antenna parameters is obtained and analysed. The results indicate that the antenna parameters have a significant effect on field coverage. The investigation in this paper offers insight into understanding and interpreting field coverage characteristics in tunnels.

Appendix

The last summation in (9) can be expanded as

$$\begin{aligned}
&\sum_{l=1}^{4}(-1)^{l+1}\,\widetilde{f}_l\left(\frac{p\pi}{2a},\frac{q\pi}{2b}\right)\exp\left(j\left(\frac{p\pi}{2a}\overline{x}_l+\frac{q\pi}{2b}\overline{y}_l\right)\right)\\
&\quad=\frac{1}{j2\pi k\left(k^2-\left(p\pi/2a\right)^2-\left(q\pi/2b\right)^2\right)}\\
&\quad\cdot\exp\left\{-\left[\frac{\left(p\pi/2ak\right)^2}{a\Delta_\perp}+\frac{\left(q\pi/2bk\right)^2}{b\Delta_\parallel}\right]z\right.\\
&\quad\left.-jz\sqrt{k^2-\left(\frac{p\pi}{2a}\right)^2-\left(\frac{q\pi}{2b}\right)^2}\right\}\sum_{l=1}^{4}(-1)^{l+1}\\
&\quad\cdot e^{j((p\pi/2a)\overline{x}_l+(q\pi/2b)\overline{y}_l)}\\
&\quad\cdot\exp\left\{-\left[\frac{p\pi/2ak-\varphi_0}{\sqrt{\sigma}\varphi_{\mathrm{BW}}}\right]^2-\left[\frac{q\pi/2bk-\theta_0}{\sqrt{\sigma}\theta_{\mathrm{BW}}}\right]^2\right\}
\end{aligned}\tag{A.1}$$

from which (12) and (13) can be obtained. The remaining summation formula in (A.1) can be further simplified by the Euler formula as follows:

$$\begin{aligned}
&\sum_{l=1}^{4}(-1)^{l+1}\,e^{j((p\pi/2a)\overline{x}_l+(q\pi/2b)\overline{y}_l)}\\
&\quad\cdot\exp\left\{-\left[\frac{p\pi/2ak-\varphi_0}{\sqrt{\sigma}\varphi_{\mathrm{BW}}}\right]^2-\left[\frac{q\pi/2bk-\theta_0}{\sqrt{\sigma}\theta_{\mathrm{BW}}}\right]^2\right\}\\
&\quad=\exp\left\{-\frac{\left(p\pi/2ak\right)^2-\varphi_0^2}{\sigma\varphi_{\mathrm{BW}}^2}-\frac{\left(q\pi/2bk\right)^2-\theta_0^2}{\sigma\theta_{\mathrm{BW}}^2}\right\}\\
&\quad\cdot\sum_{l=1}^{4}(-1)^{l+1}\,e^{j((p\pi/2a)\overline{x}_l+(q\pi/2b)\overline{y}_l)}\\
&\quad\cdot\exp\left\{\frac{p\pi\varphi_0/ak}{\sigma\varphi_{\mathrm{BW}}^2}+\frac{q\pi\theta_0/bk}{\sigma\theta_{\mathrm{BW}}^2}\right\},
\end{aligned}\tag{A.2}$$

where the second term on the right side can be expressed by

$$\begin{aligned}
&\sum_{l=1}^{4}(-1)^{l+1}\,e^{j((p\pi/2a)\overline{x}_l+(q\pi/2b)\overline{y}_l)}\\
&\quad\cdot\exp\left\{\frac{p\pi\varphi_0/ak}{\sigma\varphi_{\mathrm{BW}}^2}+\frac{q\pi\theta_0/bk}{\sigma\theta_{\mathrm{BW}}^2}\right\}\\
&\quad=e^{-j(p\pi/2a)x}\left[e^{j(p\pi/2a)x_0}-e^{-j((p\pi/2a)x_0-p\pi)}\right]\\
&\quad\cdot\exp\left(\frac{p\pi\varphi_0/ak}{\sigma\varphi_{\mathrm{BW}}^2}\right)e^{-j(q\pi/2b)y}\left[e^{j(q\pi/2b)y_0}\right.\\
&\quad\left.-e^{-j((q\pi/2b)y_0-q\pi)}\right]\exp\left(\frac{q\pi\theta_0/bk}{\sigma\theta_{\mathrm{BW}}^2}\right).
\end{aligned}\tag{A.3}$$

Substituting (A.3) into (9) and considering the summation of indexes p and q as

$$\begin{aligned}
E_r(x,y,z)&=\frac{E_t\pi^2}{4ab}\sum_{p=-\infty}^{\infty}\sum_{q=-\infty}^{\infty}e^{-j(p\pi/2a)x}\left[e^{j(p\pi/2a)x_0}\right.\\
&\quad\left.-e^{-j((p\pi/2a)x_0-p\pi)}\right]\exp\left(\frac{p\pi\varphi_0/ak}{\sigma\varphi_{\mathrm{BW}}^2}\right)\\
&\quad\cdot e^{-j(q\pi/2b)y}\left[e^{j(q\pi/2b)y_0}-e^{-j((q\pi/2b)y_0-q\pi)}\right]\\
&\quad\cdot\exp\left(\frac{q\pi\theta_0/bk}{\sigma\theta_{\mathrm{BW}}^2}\right)=\frac{E_t\pi^2}{4ab}\\
&\quad\cdot\sum_{p=-\infty}^{\infty}e^{-j(p\pi/2a)x}\left[e^{j(p\pi/2a)x_0}-e^{-j((p\pi/2a)x_0-p\pi)}\right]\\
&\quad\cdot\exp\left(\frac{p\pi\varphi_0/ak}{\sigma\varphi_{\mathrm{BW}}^2}\right)\sum_{q=-\infty}^{\infty}e^{-j(q\pi/2b)y}\left[e^{j(q\pi/2b)y_0}\right.\\
&\quad\left.-e^{-j((q\pi/2b)y_0-q\pi)}\right]\exp\left(\frac{q\pi\theta_0/bk}{\sigma\theta_{\mathrm{BW}}^2}\right)
\end{aligned}\tag{A.4}$$

then the complex exponential functions corresponding to summation of index p in (A.4) can be converted to sinusoidal functions based on Euler's formula as

$$\begin{aligned}
&\sum_{p=-\infty}^{\infty}e^{-j(p\pi/2a)x}\left[e^{j(p\pi/2a)x_0}-e^{-j((p\pi/2a)x_0-p\pi)}\right]\\
&\quad\cdot\exp\left(\frac{p\pi\varphi_0/ak}{\sigma\varphi_{\mathrm{BW}}^2}\right)
\end{aligned}$$

$$= \sum_{p=1}^{\infty} \left\{ e^{-j(p\pi/2a)x} \left[e^{j(p\pi/2a)x_0} - e^{-j((p\pi/2a)x_0 - p\pi)} \right] \cdot \exp\left(\frac{p\pi\varphi_0/ak}{\sigma\varphi_{\mathrm{BW}}^2} \right) + e^{j(p\pi/2a)x} \left[e^{-j(p\pi/2a)x_0} - e^{j((p\pi/2a)x_0 - p\pi)} \right] \cdot \exp\left(\frac{-p\pi\varphi_0/ak}{\sigma\varphi_{\mathrm{BW}}^2} \right) \right\} = \sum_{p=1}^{\infty} \left\{ e^{-j(p\pi/2a)x} e^{jp\pi} \cdot \exp\left(\frac{p\pi\varphi_0/ak}{\sigma\varphi_{\mathrm{BW}}^2} \right) - e^{j(p\pi/2a)x} \cdot \exp\left(\frac{-p\pi\varphi_0/ak}{\sigma\varphi_{\mathrm{BW}}^2} \right) \right\} \left(e^{j(p\pi/2a)x_0} e^{-jp\pi} - e^{-j(p\pi/2a)x_0} \right)$$
$$= 4\sum_{p=1}^{\infty} \sin\left(\frac{p\pi}{2a}x_0 - \frac{p\pi}{2} - j\frac{p\pi\varphi_0}{\sigma ak\varphi_{\mathrm{BW}}^2} \right) \cdot \sin\left(\frac{p\pi}{2a}x - \frac{p\pi}{2} \right). \tag{A.5}$$

Similar to (A.5), the summation corresponding to index q can be expressed as

$$\sum_{q=-\infty}^{\infty} e^{-j(q\pi/2b)y} \left[e^{j(q\pi/2b)y_0} - e^{-j((q\pi/2b)y_0 - q\pi)} \right] \cdot \exp\left(\frac{q\pi\theta_0/bk}{\sigma\theta_{\mathrm{BW}}^2} \right) = 4\sum_{q=1}^{\infty} \sin\left(\frac{q\pi}{2b}y_0 - \frac{q\pi}{2} - j\frac{q\pi\theta_0}{\sigma bk\theta_{\mathrm{BW}}^2} \right) \cdot \sin\left(\frac{q\pi}{2b}y - \frac{q\pi}{2} \right). \tag{A.6}$$

Because of the symmetry of the images, x and x_0 can be exchanged. By substituting (A.4), (A.5), and (A.6) into (11), then formula (14) can be obtained.

When the antenna pattern $F(\theta, \varphi)$ is unknown, (A.1) can been expressed as

$$\sum_{l=-\infty}^{4} (-1)^{l+1} \widetilde{f}_l\left(\frac{p\pi}{2a}, \frac{q\pi}{2b} \right) e^{j((p\pi/2a)\overline{x}_l + (q\pi/2b)\overline{y}_l)} = \frac{1}{j2\pi k\left(k^2 - (p\pi/2a)^2 - (q\pi/2b)^2 \right)} \cdot \exp\left\{ -\left[\frac{(p\pi/2ak)^2}{a\Delta_\perp} + \frac{(q\pi/2bk)^2}{b\Delta_\parallel} \right] z - jz\sqrt{k^2 - \left(\frac{p\pi}{2a}\right)^2 - \left(\frac{q\pi}{2b}\right)^2} \right\} \sum_{l=1}^{4} (-1)^{l+1} \cdot e^{j((p\pi/2a)\overline{x}_l + (q\pi/2b)\overline{y}_l)} F\left(\frac{p\pi}{2ak}, \frac{q\pi}{2bk} \right). \tag{A.7}$$

Similar to (A.5) and (A.6), the final summation for the unknown radiation pattern case can be given as

$$\sum_{p=-\infty}^{\infty} \sum_{q=-\infty}^{\infty} \sum_{l=1}^{4} (-1)^{l+1} \cdot e^{j((p\pi/2a)\overline{x}_l + (q\pi/2b)\overline{y}_l)} F\left(\frac{p\pi}{2ak}, \frac{q\pi}{2bk} \right) = \sum_{p=1}^{\infty} \sum_{q=1}^{\infty} \left[e^{j((p\pi/2a)x_0 - (p\pi/2))} - e^{-j((p\pi/2a)x_0 - (p\pi/2))} \right] \cdot \left[e^{j((q\pi/2b)y_0 - (q\pi/2))} - e^{-j((q\pi/2b)y_0 - (q\pi/2))} \right] \cdot \left[e^{-j((p\pi/2a)x - (p\pi/2))} e^{-j((q\pi/2b)y - (q\pi/2))} F_+ - e^{j((p\pi/2a)x - (p\pi/2))} e^{j((q\pi/2b)y - (q\pi/2))} F_- \right]$$
$$= 4\sum_{p=1}^{\infty} \sum_{q=1}^{\infty} \sin\left(\frac{p\pi}{2a}x_0 - \frac{p\pi}{2} \right) \sin\left(\frac{q\pi}{2b}y_0 - \frac{q\pi}{2} \right) \cdot \left[(F_- - F_+) \cos\left(\frac{p\pi}{2a}x_0 + \frac{q\pi}{2b}y_0 - p\pi \right) - j(F_- + F_+) \sin\left(\frac{p\pi}{2a}x_0 + \frac{q\pi}{2b}y_0 - p\pi \right) \right]. \tag{A.8}$$

Because of the symmetry of the images, x and x_0 can be exchanged, and then (15) can be obtained.

Competing Interests

The authors declare that they have no competing interests.

Acknowledgments

This work was supported by NSFC Projects under Grant no. 61331002 and in part by the National Key Basic Research Project under Grant no. 2013CB328903.

References

[1] C. Briso-Rodriguez, J. M. Cruz, and J. I. Alonso, "Measurements and modeling of distributed antenna systems in railway tunnels," *IEEE Transactions on Vehicular Technology*, vol. 56, no. 5, pp. 2870–2879, 2007.

[2] N. Papanikolaou, A. Spanakis, D. Apostolakis, and P. Constantinou, "Radio coverage measurements into tunnel with leaky section radiating cable," in *Proceedings of the 9th International Symposium onComputers and Communications (ISCC '04)*, pp. 714–719, Alexandria, Egypt, June 2004.

[3] A. E. Forooshani, S. Bashir, D. G. Michelson, and S. Noghanian, "A survey of wireless communications and propagation modeling in underground mines," *IEEE Communications Surveys and Tutorials*, vol. 15, no. 4, pp. 1524–1545, 2013.

[4] A. G. Emslie, R. L. Lagace, and P. F. Strong, "Theory of the propagation of UHF radio waves in coal mine tunnels," *IEEE Transactions on Antennas and Propagation*, vol. 23, no. 2, pp. 192–205, 1975.

[5] K. D. Laakmann and W. H. Steier, "Waveguides: characteristic modes of hollow rectangular dielectric waveguides," *Applied Optics*, vol. 15, no. 5, pp. 1334–1340, 1976.

[6] Y. Hwang, Y. P. Zhang, and R. G. Kouyoumjian, "Ray-optical prediction of radio-wave propagation characteristics in tunnel environments-part 1: theory," *IEEE Transactions on Antennas and Propagation*, vol. 46, no. 9, pp. 1328–1336, 1998.

[7] Y. P. Zhang, Y. Hwang, and R. G. Kouyoumjian, "Ray-optical prediction of radio-wave propagation characteristics in tunnel environments-part 2: analysis and measurements," *IEEE Transactions on Antennas and Propagation*, vol. 46, no. 9, pp. 1337–1345, 1998.

[8] M. M. Rana and A. S. Mohan, "Segmented-locally-one-dimensional-FDTD method for em propagation inside large complex tunnel environments," *IEEE Transactions on Magnetics*, vol. 48, no. 2, pp. 223–226, 2012.

[9] D.-W. Li, Y.-W. Huang, J.-H. Wang, M.-E. Chen, and Z. Zhang, "Study on the effect of radiation pattern on the field coverage in rectangular tunnel by FDTD method and point source array approximation," in *Proceedings of the International Symposium on Antennas and Propagation (ISAP '13)*, pp. 697–700, Nanjing, China, October 2013.

[10] A. V. Popov and N. Y. Zhu, "Modeling radio wave propagation in tunnels with a vectorial parabolic equation," *IEEE Transactions on Antennas and Propagation*, vol. 48, no. 9, pp. 1403–1412, 2000.

[11] R. Martelly and R. Janaswamy, "An ADI-PE approach for modeling radio transmission loss in tunnels," *IEEE Transactions on Antennas and Propagation*, vol. 57, no. 6, pp. 1759–1770, 2009.

[12] Y. P. Zhang, "Novel model for propagation loss prediction in tunnels," *IEEE Transactions on Vehicular Technology*, vol. 52, no. 5, pp. 1308–1314, 2003.

[13] Y. Huo, Z. Xu, H.-D. Zheng, and X. Zhou, "Effect of antenna on propagation characteristics of electromagnetic waves in tunnel environments," in *Proceedings of the 1st Asia Pacific Conference on Postgraduate Research in Microelectronics and Electronics (PrimeAsia '09)*, pp. 268–271, Shanghai, China, January 2009.

[14] I. B. Mabrouk, L. Talbi, M. Nedil, Y. Coulibaly, and T. Denidni, "Effect of antenna directivity on performance of multiple input multiple output systems in an underground gold mine," *IET Microwaves, Antennas and Propagation*, vol. 6, no. 5, pp. 555–561, 2012.

[15] T. Manabe, Y. Miura, and T. Ihara, "Effects of antenna directivity and polarization on indoor multipath propagation characteristics at 60 GHz," *IEEE Journal on Selected Areas in Communications*, vol. 14, no. 3, pp. 441–447, 1996.

[16] C. Zhou and J. Waynert, "The equivalence of the ray tracing and modal methods for modeling radio propagation in lossy rectangular tunnels," *IEEE Antennas and Wireless Propagation Letters*, vol. 13, pp. 615–618, 2014.

[17] C. Zhou, J. Waynert, T. Plass, and R. Jacksha, "Attenuation constants of radio waves in lossy-walled rectangular waveguides," *Progress in Electromagnetics Research*, vol. 142, pp. 75–105, 2013.

[18] Z. Sun and I. F. Akyildiz, "Channel modeling and analysis for wireless networks in underground mines and road tunnels," *IEEE Transactions on Communications*, vol. 58, no. 6, pp. 1758–1768, 2010.

[19] J. D. Kraus, *Antennas*, McGraw-Hill, Singapore, 2nd edition, 1988.

[20] D. G. Dudley, M. Liénard, S. F. Mahmoud, and P. Degauque, "Wireless propagation in tunnels," *IEEE Antennas and Propagation Magazine*, vol. 49, no. 2, pp. 11–26, 2007.

[21] J. M. Molina-Garcia-Pardo, M. Lienard, P. Degauque, D. G. Dudley, and L. Juan-Llacer, "Interpretation of MIMO channel characteristics in rectangular tunnels from modal theory," *IEEE Transactions on Vehicular Technology*, vol. 57, no. 3, pp. 1974–1979, 2008.

[22] S. Bashir, "Effect of antenna position and polarization on UWB propagation channel in underground mines and tunnels," *IEEE Transactions on Antennas and Propagation*, vol. 62, no. 9, pp. 4771–4779, 2014.

[23] J. A. Castiblanco, D. Seetharamdoo, M. Berbineau, M. Ney, and F. Gallee, "Determination of antenna specification and positioning for efficient railway communication in tunnels of arbitrary cross section," in *Proceedings of the 11th International Conference on ITS Telecommunications (ITST '11)*, pp. 678–683, IEEE, St. Petersburg, Russia, August 2011.

[24] J.-M. Molina-Garcia-Pardo, M. Lienard, P. Degauque, E. Simon, and L. Juan-Llacer, "On MIMO channel capacity in tunnels," *IEEE Transactions on Antennas and Propagation*, vol. 57, no. 11, pp. 3697–3701, 2009.

[25] Z. Sun and I. F. Akyildiz, "Optimal MIMO antenna geometry analysis for wireless networks in underground tunnels," in *Proceedings of the IEEE Global Telecommunications Conference (GLOBECOM '09)*, pp. 1–6, Honolulu, Hawaii, USA, December 2009.